

Time-resolved detection of individual electrons in a quantum dot

R. Schleser,^{a)} E. Ruh, T. Ihn, and K. Ensslin
Solid State Physics Laboratory, ETH Zürich, 8093 Zürich, Switzerland

D. C. Driscoll and A. C. Gossard
Materials Department, University of California, Santa Barbara, California 93106

(Received 12 April 2004; accepted 22 June 2004)

We present measurements on a quantum dot and a nearby, capacitively coupled, quantum point contact used as a charge detector. With the dot being weakly coupled to only a single reservoir, the transfer of individual electrons onto and off the dot can be observed in real time in the current signal from the quantum point contact. From these time-dependent traces, the quantum mechanical coupling between dot and reservoir can be extracted quantitatively. A similar analysis allows the determination of the occupation probability of the dot states. © 2004 American Institute of Physics. [DOI: 10.1063/1.1784875]

The electronic occupation in semiconductor quantum dots can be read out using a quantum point contact (QPC).¹ Quantum dots are proposed as scalable spin qubits in a future quantum information processor² and the read-out could be implemented by a QPC detector. Experiments using a radio-frequency single-electron transistor resulted in a high bandwidth real-time read-out of a quantum dot's charge state.³ Theoretical considerations on dephasing^{4,5} have given evidence that a higher quantum measurement efficiency can be obtained using a detector without any internal degrees of freedom, such as, e.g., a QPC containing a single mode. Recent investigations using QPCs as charge detectors were performed on double^{6,7} and single^{8,9} quantum dots, all using dc or lock-in techniques that average over many electrons passing through the dot. Very recently, real-time charge read-out measurements on a split-gate defined structure were reported.¹⁰

In this letter, we present measurements detecting single electrons in real time using a QPC charge detector, in a circuit created entirely by surface probe lithography.¹¹⁻¹³ The structure consists of a quantum dot and a nearby, electrostatically coupled QPC [see Fig. 1(a)]. It is written on a GaAs/Al_{0.3}Ga_{0.7}As heterostructure, containing a two-dimensional electron gas (2DEG) 34 nm below the surface as well as a backgate 1400 nm below the 2DEG, isolated from it by a layer of low-temperature-grown (LT)-GaAs. Negative voltages were applied to the surrounding gates (G1, G2, S_{QPC}, D_{QPC}, the latter two also containing the charge detection circuit), and to the back gate, to reduce the charge on the dot and close its tunnel barriers. A voltage applied to gate P was used to tune the detector QPC to a regime where it is sensitive to the charge on the dot.

All measurements were performed in a dilution refrigerator with a base temperature of 80 mK. A small bias voltage $V_{\text{bias,dot}}=10 \mu\text{V}$ was symmetrically applied across the dot between source (S_{QD}) and drain (D_{QD}). In a regime where both barriers are open and a transport current through the dot is measurable, the example traces in Figs. 1(b) and 1(c) were measured, showing the correlation between the Coulomb peaks in the transport current [Fig. 1(b)] and the corresponding kinks in the conductance vs gate voltage

curve of the QPC [Fig. 1(c)]. For later measurements, a compensation voltage $V_P=aV_{G1}+bV_{G2}$ was applied to the gate P, with constants a and b chosen such as to keep the charge detection circuit in a regime of almost constant sensitivity. The sensitivity of our atomic force microscopy (AFM)-defined circuit is comparable to similar setups realized by electron-beam lithography defined split-gate devices.^{6,7}

The following measurements were performed with one tunnel barrier (the one near the drain contact) completely closed and the other one tuned to a very low electron transition rate, of the order of only a few electrons per second.

Figure 2(a) shows a section of a measurement of the QPC detector's conductance versus two different gate voltages, where each vertical or horizontal trace can be thought of as being similar to Fig. 1(c). Each step corresponds to an electron being transferred onto the dot. Towards lower values of V_{G2} (see marked region), the smooth behavior of the step transforms to a discrete appearance where only two possible values for the QPC conductance are observed.

In the following, we present time-dependent traces of the QPC's conductance. All traces were recorded using an oscilloscope at a sampling frequency of 250 Hz. Each trace had a length of 9 s. For a time-dependent measurement near a step in the QPC's conductance, one observes that the system switches randomly between the two states [Fig. 2(b)]. The

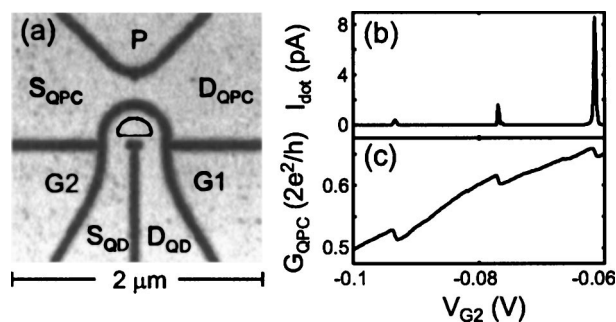


FIG. 1. (a) AFM micrograph of the structure with designations of gates: Source (S) and drain (D) of the quantum dot and the QPC used as a charge detector; lateral gates G1 and G2 to control the coupling of the dots to the reservoirs; Plunger gate (P) to tune the QPC detector. (b) Example measurement of the current through the dot. (c) Simultaneous measurement of the conductance through the QPC, where each step corresponds to a change of the dot's charge by one electron.

^{a)}Electronic mail: schleser@phys.ethz.ch

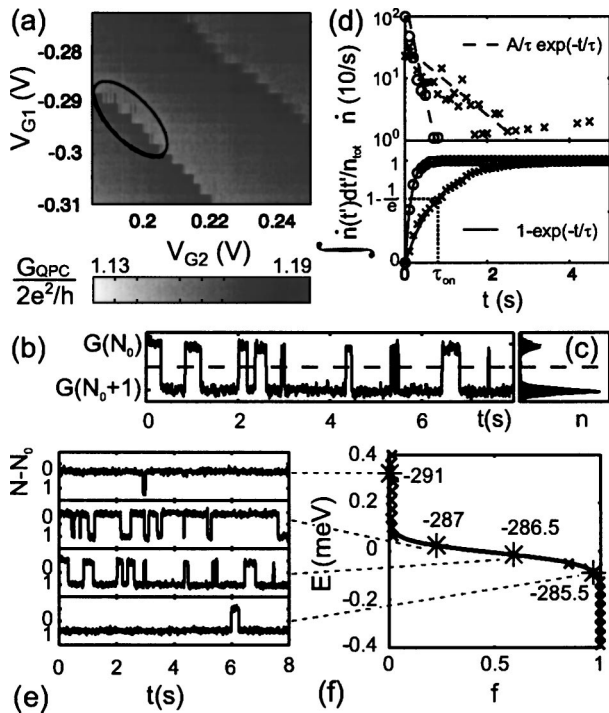


FIG. 2. (a) Measurement of the QPC's conductance versus V_{G1} and V_{G2} . Toward lower values of V_{G2} (see, e.g., inside the black ellipse), the smooth, washed out appearance of the step in conductance is replaced by a discrete switching behavior with only two possible states. The time between individual measured points was about 2 s, the integration time of the (dc) measurement 0.2 s. (b) Single oscilloscope trace of the QPC's conductance vs time. The dot was tuned to a point near a step in the QPC's conductance. (c) Histogram of the data in plot (b) and 19 similar sweeps. (d) The upper graph shows a histogram of the distribution of dwell times of the electron both inside (o) and outside (x) the dot. A correction was applied to account for the finite size of the oscilloscope's measurement intervals. The bin size was chosen to be 0.1 s, data were taken from 20 sweeps of 9 s each. The lower graph shows the time-integrated, normalized distribution. Dashed and solid lines represent exponential fits to the data with the same parameters τ_{on} , τ_{off} for both graphs. (e) Changing the voltage V_{G1} (at a constant $V_{G2}=185$ mV) changes the dot's electrochemical potential and allows a transition from the N electron state to the $N+1$ electron state. In the oscilloscope traces, this is seen as a change in the relative occupancy of the two possible QPC states. (f) Distribution $f(E)$ extracted from oscilloscope traces (where for every point, 20 traces each of length 9 were taken into account). The data points marked by large asterisks correspond directly to the traces shown in (b). These asterisks are labeled by the corresponding gate voltage V_{G1} in mV.

difference between the two values corresponds to the observed step height in Fig. 2(a) in the parameter range featuring a smooth transition. This allows a discrimination between charging events on the dot and other possible sources of switching events.

The upper plot in Fig. 2(d) shows an example for the distribution of times the systems spend in both states. The lower plot shows the integrated normalized distribution representing the probability that after a certain time the system has changed its state at least once. Exponential fits $\exp(-t/\tau)$ agree well with the data and suggest that: (1) The behavior of the system does not depend on its history and (2) that a single-energy level in the dot contributes to charging.

From the exponential fits, mean times τ_{on} for an electron jumping on the dot and τ_{off} for an electron jumping off the dot can be obtained. The same numbers can be extracted by counting the transitions per time interval f_{trans} during a time sweep and determining the fractions p_{on} and p_{off} of the total time the system spends in each of the two states [see histo-

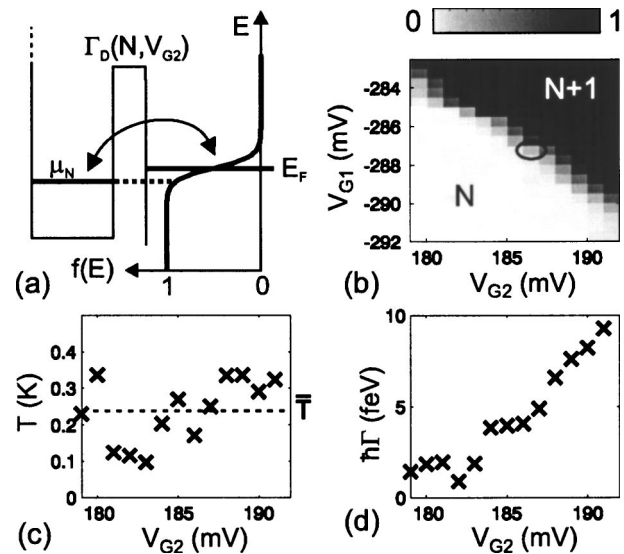


FIG. 3. (a) Model for the transfer of individual electrons between a single reservoir and a quantum dot. The tunnel coupling is assumed to depend on the single-level state N and can be tuned via the voltage V_{G2} . (b) Grey scale plot of the relative occupancy p_{on} of the dot. Each point is calculated from 20 oscilloscope traces, each 9 s long. The section corresponds roughly to the marked range of Fig. 2(a). Due to a minor charge rearrangement, however, the voltage ranges are not exactly the same. The ellipse marks the point where the statistical analysis of dwell times [Fig. 2(d)] was applied. This measurement was performed with the QPC containing more than one mode. (c) Temperature extracted from the data in (a) using a fit of the Fermi function [see Fig. 2(f)] for every value of the gate voltage V_{G2} . (d) Coupling strength Γ to the leads extracted from the same set of data as (a) and (b). As expected, Γ increases with V_{G2} .

gram in Fig. 2(c)). It follows that $\tau_{on}=p_{on}/(f_{trans}/2)$ and $\tau_{off}=p_{off}/(f_{trans}/2)$.

By changing the gate voltage V_{G1} , the electrochemical potential in the dot can be modified. Figure 2(e) shows a series of time-dependent traces for different V_{G1} . Using the lever arm α_{G1} , the gate voltage can be converted to an energy scale $E=-\alpha_{G1}V_{G1}$, so that a distribution $f(E)\equiv p_{on}(E)$ is obtained [see Fig. 2(f)]. To reduce the statistical error, 20 time sweeps have been analyzed for every data point shown.

In a regime where only one tunnel barrier is open, no finite bias transport measurements are possible which would allow the determination of the exact value of α_{G1} . Its value is therefore obtained from the peak spacing by assuming a charging energy of the dot $E_c=2$ mV, determined from finite bias transport measurements performed in a more open regime of the dot. This method yields $\alpha_{G1}\approx 0.075$ eV/V, a value that was used in Fig. 2(f) and 3(c). Considering that, at lower electron numbers, E_c tends to increase due to the reduction in size of the dot, the energy and temperature values to be determined below [see Figs. 2(f) and 3(c)] are to be considered an upper bound.

Motivated by the experimental findings and their statistical properties, we interpret our results using the model depicted in Fig. 3(a), which shows a single-energy level in a quantum dot which can be aligned with respect to the Fermi level of the reservoir, from which it is separated by a tunable tunnel barrier. The lower conductance in the QPC [see Fig. 2(b)] corresponds to the state where an electron is on the dot, due to the capacitive coupling of the dot to the QPC. A similar scheme was used in an experiment using a single-electron transistor as a detector.³ A more sophisticated analy-

sis considering more than one level in the dot can be performed using the theory by Beenakker.¹⁴

Assuming that an electron is on the dot, the mean rate at which it will leave the dot is

$$\tau_{\text{off}}^{-1} = \Gamma \times (1 - f(\mu_N)), \quad (1)$$

where τ_{off} is the average time interval the dot stays in the $(N+1)$ electron state, μ_N is the electrochemical potential for the addition of the N th electron, $f(E)$ is the distribution function in the reservoir, and Γ is the coupling between the level and the reservoir. Physically, the value of Γ accounts for the strength of tunnel barriers, wave function overlap, and the lead's density of states (assumed to be constant over the relevant energy interval). Correspondingly, the rate for electrons to tunnel on an (initially empty) dot is

$$\tau_{\text{on}}^{-1} = \Gamma \times f(\mu_N). \quad (2)$$

It follows from Eqs. (1) and (2) that

$$\Gamma = \tau_{\text{off}}^{-1} + \tau_{\text{on}}^{-1} \quad (3)$$

$$\text{and } f(\mu_N) = \tau_{\text{off}} / (\tau_{\text{off}} + \tau_{\text{on}}). \quad (4)$$

This means that we are able to determine the tunnel coupling Γ_N of an individual energy level to a single reservoir as well as the energy distribution $f(E)$ of the lead.

In Fig. 2(f), the solid line represents a fit using the Fermi distribution $f(E) = 1/(1 + \exp(-E/k_B T))$, from which a temperature $T \approx 150$ mK can be extracted.

In the following, we present data in a more extended parameter regime. Figure 3(b) shows a plot of the extracted distribution function $f(E)$ versus the two gate voltages V_{G1} and V_{G2} . For each scan in the direction of V_{G1} , a fit using the Fermi distribution was made. The resulting temperature values are represented in Fig. 3(c), the mean value being slightly above 200 mK. The origin of the scattering of T values in Fig. 3(c) remains to be investigated, since it cannot be assigned entirely to uncertainties in the fitting procedure or lack of data points.

The numerical extraction of the parameter Γ is most reliable near the transition. Γ was therefore determined where

$f(E)$ was closest to $1/2$. The resulting curve is shown in Fig. 3(d). Over the range presented, Γ changes by roughly one order of magnitude. Further reducing V_{G2} by only a few ten mV leads to a further increase of the observed times between switching events (of the order of minutes and more). This is in accordance with recent observations of long dwell times of electrons on a single¹⁵ or double⁷ dot.

We have reported on the real-time charge read-out of a quantum dot using a QPC, both defined by AFM lithography. We estimate that amplifier and cabling bandwidth as well as the sensitivity can be improved to reach read-out frequencies in the MHz range (see also Ref. 10).

The authors gratefully acknowledge financial support from the Swiss National Science Foundation and the NCCR "Nanoscale Science."

¹M. Field, C. G. Smith, M. Pepper, D. A. Ritchie, J. E. F. Frost, G. A. C. Jones, and D. G. Hasko, *Phys. Rev. Lett.* **70**, 1311 (1993).

²D. Loss and D. P. DiVincenzo, *Phys. Rev. A* **57**, 120 (1998).

³W. Lu, Z. Ji, L. Pfeiffer, K. W. West, and A. J. Rimberg, *Nature (London)* **423**, 422 (2003).

⁴S. Pilgram and M. Büttiker, *Phys. Rev. Lett.* **89**, 200401 (2003).

⁵A. A. Clerk, S. M. Girvin, and A. D. Stone, *Phys. Rev. B* **67**, 165324 (2003).

⁶J. M. Elzerman, R. Hanson, J. S. Greidanus, L. H. W. van Beveren, S. De-Franceschi, L. M. K. Vandersypen, S. Tarucha, and L. P. Kouwenhoven, *Phys. Rev. B* **67**, 161308 (2003).

⁷S. Gardelis, C. G. Smith, J. Cooper, D. A. Ritchie, E. H. Linfield, Y. Jin, and M. Pepper, *Phys. Rev. B* **67**, 073302 (2003).

⁸R. Hanson, B. Witkamp, L. M. K. Vandersypen, L. H. W. van Beveren, J. M. Elzerman, and L. P. Kouwenhoven, *Phys. Rev. Lett.* **91**, 196802 (2003).

⁹J. Elzerman, R. Hanson, L. W. V. Beveren, L. Vandersypen, and L. Kouwenhoven, *Appl. Phys. Lett.* **84**, 4617 (2004).

¹⁰J. Elzerman, L. Vandersypen, R. Hanson, I. Vink, L. W. van Beveren, and L. Kouwenhoven (unpublished).

¹¹R. Held, S. Lüscher, T. Heinzel, K. Ensslin, and W. Wegscheider, *Appl. Phys. Lett.* **75**, 1134 (1999).

¹²S. Lüscher, A. Fuhrer, R. Held, T. Heinzel, K. Ensslin, and W. Wegscheider, *Appl. Phys. Lett.* **75**, 2452 (1999).

¹³R. Nemutudi, M. Kataoka, C. J. B. Ford, N. J. Appleyard, M. Pepper, D. A. Ritchie, and G. A. C. Jones, *J. Appl. Phys.* **95**, 2557 (2004).

¹⁴C. W. J. Beenakker, *Phys. Rev. B* **44**, 1646 (1991).

¹⁵J. Cooper, C. G. Smith, D. A. Ritchie, E. H. Linfield, Y. Jin, and H. Launois, *Physica E (Amsterdam)* **6**, 457 (2000).